 CMC, vol.10, no.3, pp.217-228, 2009

Effect of Process Parameters on Laser Surface Hardening of Plain Carbon Eutectoid Steel

S. Mukherjee[1], S. Chakraborty[2] and I. Manna[1,3]

Abstract: Influence of power density and interaction time for austenitisation during laser surface hardening of plain carbon eutectoid steel has been investigated. The analysis involves numerical prediction of thermal and solute diffusion profiles and thereby, the time needed for homogenization of austenite for different processing conditions. Experimental results provide qualitative validation.

Keywords: Modeling, laser surface hardening, steel, austenite, homogenization

1 Introduction

Laser assisted surface hardening (LSH) of steel is a well established surface engineering technique that allows rapid, selective and convenient hardening of the surface of steel components [Dutta Majumdar and Manna (2003); Molian (1989); Pantelis et al (2002); Senthil et al (1999); Grum and Kek (2004); Shin et al (2007); Basu et al (2007); Pashby et al (2003)]. The process involves austenitization, followed by rapid quenching of the near surface region of the steel component, without melting or changing composition. In this process, development of the desired microstructure and mechanical properties critically depends on the thermal cycle comprising the heating/cooling rates and exposure time. While rapid cooling is a primary requirement of hardening to suppress initiation of pearlitic transformation, dissolution of carbides and formation of homogeneous austenite are also essential to ensure uniformity in microstructure and surface hardening of the component after LSH. Hence, a suitable choice of process parameters, such as power density and interaction time, is important to ensure the necessary heating rate, time for dissolution of carbides and homogenization of austenite, without involving any unwarranted overheating/oxidation. In the present contribution, we intend to numerically simulate the process of austenitization during LSH of eutectoid plain

[1] Metallurgical and Materials Engineering Department, IIT Kharagpur, India
[2] Mechanical Engineering Department, IIT Kharagpur, India
[3] Correspondence to: imanna@metal.iitkgp.ernet.in

carbon steel and determine the necessary process parameters for obtaining homogeneous austenite, prior to quenching or martensitic transformation. We also aim to study the affect of prior microstructure (inter-lamellar spacing) on the minimum time needed for homogenization of austenite without compromising with the intended microstructure and mechanical properties of the component after LSH.

2 Mathematical Model

2.1 Modeling the thermal problem

For modeling the heat transfer during LSH, a continuous-wave laser source is assumed to scan over the component with a flat surface at a constant speed u_{scan} relative to the component, along a given direction. Only a part of the incident energy from the laser beam is converted into lattice heat to subsequently cause austenitization. Once the laser source moves away, the heated layer undergoes self-quenching and consequent microstructural changes or hardening.

In order to predict the degree of cementite dissolution and homogenization of austenite in the course of laser assisted heating preceding self-quenching, the thermal profile in the laser irradiated zone is first determined by numerical solution of the transient three-dimensional thermal energy conservation, see Eq.1, in a moving reference frame attached to the laser source (which is moving along negative x direction), as follows [Sarkar and Chakraborty (2002)]:

$$\partial(\rho cT)/\partial t = \nabla(k\nabla T) - \partial(\rho u_{scan} cT)/\partial x \tag{1}$$

where ρ is the density, c is the specific heat, k is the thermal conductivity, u_{scan} is the laser scanning speed and T is the temperature reached in the time elapsed t.

Eq. 1 is subjected to the following boundary conditions for numerical solution:

2.1.1 Top Surface

A Gaussian heat flux distribution is assumed at the top surface, which is given by

$$q''(r) = q\exp(-r^2/r_q^2)/\pi r_q^2 \tag{2}$$

Here, q'' is the heat flux, q is the incident laser power irradiating the component, r_q is the half width of the beam and r is the radial distance from the axis of the laser source. Based on the above, we may write the thermal boundary conditions at the top surface. By considering heat losses due to convection and radiation, Eq. 2 reduces to:

$$-q''(r) + h(T - T_\infty) + \sigma_e \varepsilon (T^4 - T_\infty^4) = -k(\partial T/\partial y)_{top}, \tag{3}$$

where, y is the direction normal to the laser irradiation, h the convective heat transfer coefficient, σ_e the Stefan-Boltzmann constant, ε the emissivity of the top surface and T_∞ the ambient temperature.

2.1.2 Side faces

The four side faces are subjected to the following convective heat transfer boundary condition:

$$-k(\partial T/\partial n)_{wall} = h(T - T_\infty), \tag{4}$$

where, n is in the direction of the outward normal of the concerned side face.

2.1.3 Bottom Face

The bottom face is assumed to be insulated; i.e.

$$(\partial T/\partial y)_{bottom} = 0 \tag{5}$$

2.1.4 Initial Conditions

The initial conditions appropriate to model the problem are as follows
at $t = 0$, $T = T_\infty = 298$ K

2.2 Modeling of the species transport

The microstructure of plain carbon eutectoid steel comprises only pearlitic colonies with a characteristic (statistically constant) inter-lamellar spacing. Thus, austenitization involves transformation of ferrite to austenite and dissolution of cementite in the latter followed by solute redistribution and homogenization through diffusion down the chemical potential gradient up to the bulk composition. Earlier, several studies were conducted on modeling the eutectoid transformation in steels [Jacot et al (1998); Speich et al (1981); Garcı'a de Andre's et al (1998); Akbay et al (1994); Jacot and Rappaz (1998); Roósz et al (1983); Atkinson et al (1995); Gaude-Fugarolas and Bhadeshia (2003); Brooks (1992); Estay et al (1984); Palmer and Elmer (2005); Roberts and Mehl (1943); Speich and Szirmae (1969); Judd and Paxton (1968); Hillert et al (1971); Caballero et al (2000); Mioković et al (2006); Roy and Manna (2000); Patwa and Shin (2007)]. Kinetics of such ferrite to austenite transformation and subsequent homogenization has been modeled [C. Garcı'a de Andre's, F.G. Caballero, C. Capdevila and H.K.D.H. Bhadeshia (1998)] using modified Avrami equation applicable for non-isothermal condition, based on previous work done for isothermal conditions [A. Roósz, Z. Gácsi and E.G. Fuchs (1983)]. It may be noted here that homogenizing a single

colony in eutectoid steel is essentially the same as that for the whole sample due identical microstructure of lamellar aggregate. In the present problem concerning homogenization of dissolved cementite, the distance between two adjacent cementite lamellae is considered as the characteristic diffusion length. The initial exercise involves calculation of the time for austenite formation from the model stated above [Garcı'a de Andre's et al (1998)] under a specific heating rate (predicted by our thermal model). Thereafter, the time required by carbon to diffuse to the centre of the inter-lamellar region from its periphery is calculated by solving the following transient species diffusion Eq. 6:

$$\partial C/\partial t = D(\partial^2 C/\partial^2 x') \tag{6}$$

Here, x' is the local co-ordinate direction signifying the dominant direction of carbon diffusion between two lamellae, C is the local concentration of carbon and D is the corresponding mass diffusion coefficient. Finally, sum total of the superheating time and local diffusion time yields an estimate of the homogenization time required for the sample. It can be noted here that Eq.6 is solved under the following boundary conditions:

(i) At the boundary of the inter-lamellar region

$$m' = -D(\partial C/\partial x') \tag{7}$$

where, m' is the mass flux of carbon at the boundary.

(ii) In between two adjacent cementite lamellae due to spatial symmetry

$$\partial C/\partial x = 0. \tag{8}$$

It can be noted here that the thermally activated diffusion coefficient D, considered in the present model, is expressed as:

$$D = D_0 exp(-Q/(RT)) \tag{9}$$

where, D_0 is the pre-exponential factor, Q the activation energy and R the gas constant. Equation (9) provides the necessary coupling between the governing differential equations (1) and (6), through the local temperature T prevailing at the concerned time instant under consideration. As far as the initial concentration distribution is concerned, a carbon concentration of C_0 (6.67 wt%), that is the equilibrium carbon concentration in cementite, is assumed to prevail over a distance d_0 from the periphery, which is half the thickness of the cementite sheet. The remaining portion of the inter-lamellar region has a concentration C_0' which corresponds to the carbon concentration in α-ferrite.

2.3 Numerical Procedure

The governing differential equations, coupled with appropriate initial and boundary conditions are solved numerically using a fully implicit finite volume technique [Sarkar and Chakraborty (2002)]. The resultant system of linear algebraic equations is solved using a tri-diagonal matrix algorithm (TDMA) [Patankar (1980)] or its multi-dimensional extension, as required for the pertinent simulation. For iterative solution of the thermal problem, convergence in inner iterations is obtained on the basis of method of relative error and overall energy balance, with a predetermined tolerance of 0.001.

2.3.1 Choice of Grid Size and Time Steps

In LSH, the presence of an intense heat flux at the laser exposed surface leads to large temperature gradients in the vicinity of laser source. Furthermore, the whole operation takes place in a very small interval of time (typically in a few milliseconds). Therefore, a judicious choice of grid size and time step for computations is of paramount importance for numerical stability and accurate predictions of evolution of field variables.

For the thermal problem, a time step of 0.001s is used, and a $55\times55\times55$ grid system is chosen to discretize a domain of size $20\text{mm}\times8\text{mm}\times3\text{mm}$. For the species transport problem, a time step of 0.00002 s is used. The inter-lamellar spacing (λ) considered for calculations are 0.1, 1 and 10 μm. The specific interface area of pearlitic colonies for the modeling of phase transformation has been taken to be 1295 mm^{-1}. The grid size considered for the calculation of the concentration profile is $\lambda/400$. Other thermo-physical properties used for the present study are taken from [Sarkar and Chakraborty (2002); Brandes (1992)].

3 Results and Discussion

In the current section we shall discuss the effect of laser parameters on the temperature profile generated and its impact on the resulting LSH operations.

Fig. 1 shows the temperature profile generated for continuous wave (CW) CO_2 laser irradiation on plain carbon eutectoid steel, on the sample surface, with different combinations of power density (P) and interaction time (t_i). While the temperature increases with time, the degree of increase depends upon the concerned laser parameters. At a given time, the higher the P or t_i, the greater the temperature reached under comparable conditions of P and t_i. Accordingly, both the peak temperature (T_{peak}) and the time to reach $T_{peak}(t_{peak})$ increases as P and t_i increase (or overall thermal energy input increases). These results are in accordance with an earlier work on microstructural evolution in one dimensional heat flow during laser

surface alloying [Dutta Majumdar et al (2002)].

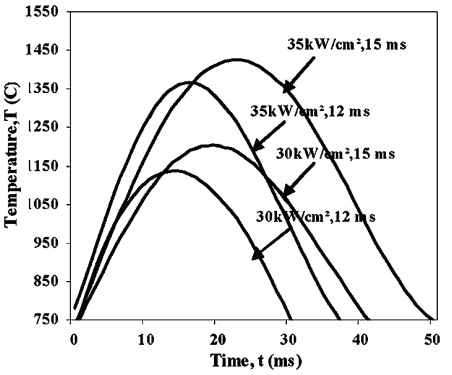

Figure 1: Variation of surface temperature with time for different LSH parameters

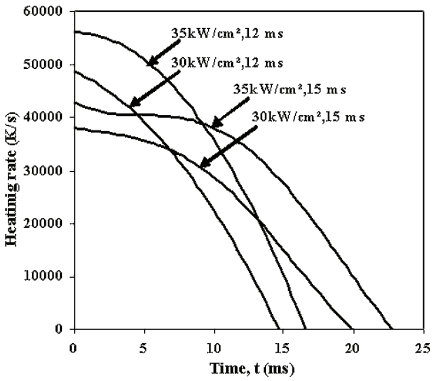

Figure 2: Variation of surface heating rate as a function of time for different combinations of P and t_i

Fig. 2 shows that the heating rate, like the absolute temperature, depends upon the concerned laser parameters. At a given time, the greater the value of P or t_i, the greater the heating rate under comparable conditions. Thus, Fig. 2 and 3 demonstrate that higher P and/or t_i enable a faster heating, a higher T_{peak} and greater thermal gradient ($\mathrm{d}T/\mathrm{d}z$) for identical time of irradiation. Incident laser energy is converted into lattice heat up to a certain depth (z) below the surface following an exponential law, depending upon thermo-physical properties of steel.

Fig. 3 shows the effect of laser parameters on temperature at different levels of z. Step gradients of temperature, established over a thin layer of the lased material, are conspicuous from the above figure. From the above plot we can observe the hardened depth achieved would be around 0.25 mm as the temperature beyond this point is not sufficient for austenisation.

Fig. 4 shows the corresponding variation of heating rate as a function of depth for different laser parameters. It may be noted that both temperature profile and heating rates at a given z are proportional to the incident power density.

The nucleation and growth of austenite form pearlitic colonies is modeled by adopting the Avrami equation for non-isothermal heating. Following this initial stage of nucleation and growth, the remaining time is required only for homogenization of austenite, particularly in the case laser surface hardening with high heating rates, by diffusion of dissolved carbon down the chemical potential gradient. It may be noted the homogenization time would principally depend upon the prior microstructural

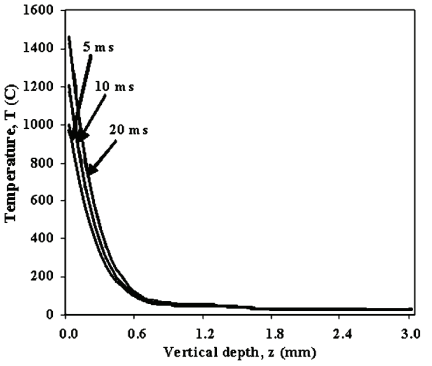

Figure 3: Variation of temperature as a function of vertical depth from the top surface for a given P (35 kW/cm^2) and varying t_i

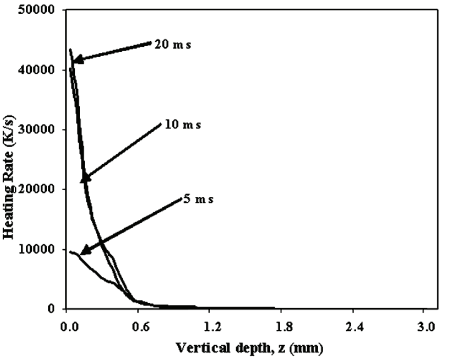

Figure 4: Variation of heating rate as a function of depth for a given P (35 kW/cm^2) and varying t_i

features (interlamellar spacing) and process parameters (laser power and interaction time).

The distribution of carbon as a function of distance from a former cementite lamella during transient heating is determined by numerical solution of Eq. 6. Under this non-isothermal condition of transient heating, dissolution and solute transport are computed for infinitesimally small time steps of one microsecond at a given temperature. Accordingly, the time taken to homogenize austenite (such that the average composition in austenite equals the initial composition of the steel) austenite following dissolution of cementite increases with decrease in heating rate. However, the temperature (T_{hom}) or the time (t_{hom}) for homogenization increases with increase in diffusion distance or inter-lamellar spacing (λ). Fig. 5 shows the effect of prior microstructure on the time for homogenization. The observations are in agreement with the existing theoretical knowledge.

It can be inferred from the above results that if the homogenization time is large or greater than the period of heating, the sample will not be homogenized and the resultant hardened microstructure will be non-uniform.

To validate the mathematical prediction, LSH experiments were performed with plain-carbon hypo-eutectoid steel at a laser power of 1.5 kW with varying beam speeds and focal offset (distance between the sample surface and laser focus). The resulting microstructure was analyzed using scanning electron microscope (SEM) and X-ray diffraction (XRD). From the microstructure of the pearlitic regions revealed under the SEM, it is apparent that inadequate thermal energy input (or in-

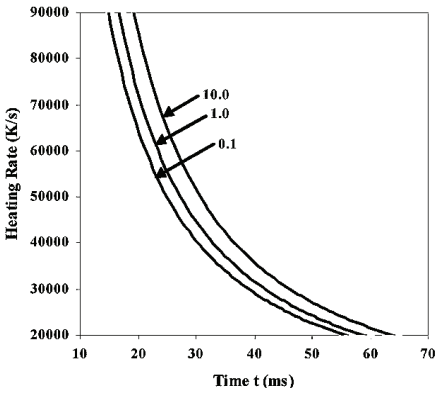

Figure 5: Effect of variation of P and t_i on the resultant heating rate for different values of λ

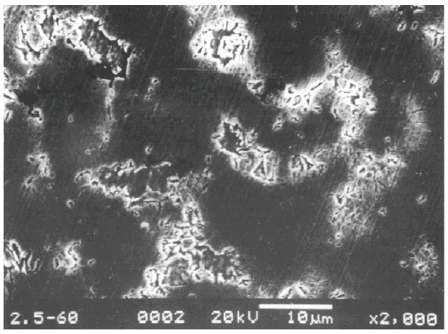

Figure 6: SEM micrograph showing incomplete and non-uniformly hardened microstructure following LSH of a plain-carbon steel with laser power of 1.5 kW and u_{scan} = 600 mm/min

adequate P or t_i) indeed results into incomplete homogenization of the pearlitic colonies (Fig. 6). From the XRD analysis, it can be seen that the percentage of retained austenite following LSH is a function of process parameters, as the LSH parameters directly affect the quenching rate and hence the amount of retained austenite. Fig. 7 and 8 show the XRD plots obtained after LSH with identical LSH parameters except the distance between the laser beam focus and substrate surface. It is apparent that the amount of retained austenite is greater in the sample after LSH with greater distance between the beam-focus and substrate-surface and hence smaller power density (Fig. 8) than that after LSH with smaller defocusing distance (Fig. 7). Relatively smaller energy input in the former case is responsible for inhomogeneous distribution of carbon after dissolution of cementite and retention of austenite due to stabilization during subsequent self-quenching.

4 Conclusion

The following inferences can be drawn from the results of present numerical simulation:

1. The peak temperature increases with increase in power density and interaction time. The time taken to reach the peak temperature also increases with interaction time for comparable values of power density.

2. The rate of increase of temperature increases with decrease in interaction time or increase in beam scanning speed.

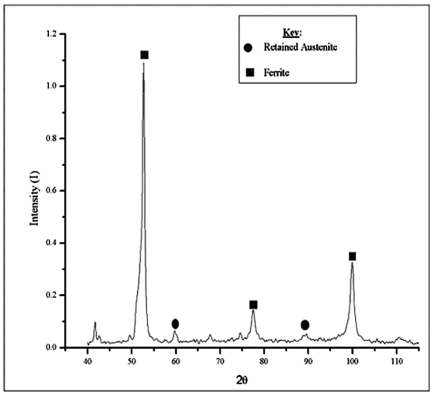

Figure 7: XRD plot following LSH with laser power of 1.5 kW, u_{scan}= 600 mm/min with the laser beam focus located 80 mm above the substrate surface

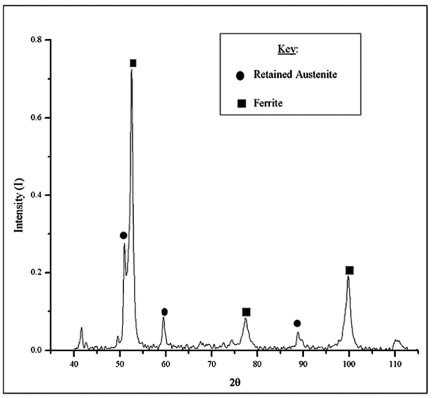

Figure 8: XRD plot following LSH with laser power of 1.5 kW, u_{scan}= 600 mm/min with the laser beam focus located 100 mm above the substrate surface

3. The effective hardening depth is around 0.25 mm beyond which sufficient energy is not converted into lattice heat to induce the hardening transformation.

4. The time required for homogenization of austenite increases with an increase in inter-lamellar spacing in the pearlite colony due to the increase in effective diffusion distance.

5. The time required for homogenization increases with decreasing power density and interaction time.

6. A critical combination of power density and interaction time is required to obtain uniform hardening by LSH. The increase in incident energy can be effective up to a limited extent, beyond which, oxidation or melting occurs.

Acknowledgement: The authors are grateful to Prof J. Estrin and Dr R Galun (IWW, Technical University of Clausthal, Germany) for helping with the experiments on LSH. Partial financial support to I.M. from the DST-NSF (RPO-131) and CSIR is gratefully acknowledged.

References

Akbay, T.; Reed R. C.; Atkinson, C. (1994): Modeling of Reaustenitisation from ferrite/cementite mixtures in Fe-steels. *Acta Metall.*, vol. 47, pp. 1469-1480.

Atkinson, C.; Akbay, T.; Reed R.C. (1995): Theory of reaustenitisation from ferrite/cementite in Fe-C-X steels. *Acta Metall.*, vol. 43, pp. 2013-2031.

Basu, A.; Chakraborty, J.; Shariff, S.M.; Padmanabham, G.; Joshi, S.V.; Sundararajan, G.; Dutta M.J.; Manna, I. (2007): Laser surface hardening of austempered (bainitic) ball bearing steel. *Scripta Materialia*, Vol. 56, no. 10, pp. 887-890.

Brandes, E.A. (1992): *Smithells metals reference book* (7th ed), Butterworth-Heinemann, Oxford.

Brooks, C.R. (1992): *Principles of the austenitization of steels*, Elsevier Applied Science, London.

Caballero, F.G.; Capdevila, C.; García de Andrés, C. (2000): Influence of Scale Parameters of Pearlite on the Kinetics of Non-Isothermal Pearlite-to-Austenite Transformation in an Eutectoid Steel. *Scripta Mater.*, vol. 42, pp. 1159.

Dutta Majumdar, J.; Manna, I. (2003): Laser processing of Materials. *Sadhana*, vol. 28, pp. 495-562.

Dutta Majumdar, J.; Mordike, B.L.; Galun, R.; Manna, I. (2002): Improving Wear and Corrosion Resistance of Mg by Laser Surface Alloying with Mn + Al. *Lasers in Engineering*, vol. 12, pp. 147-169.

Estay, S.; Chengji L.; Purdy, G.R. (1984): Direct Observations of the $\alpha \rightarrow \gamma$ Transformation at Different Input Powers in the Heat-Affected Zone of 1045 C-Mn Steel Arc Welds Observed by Spatially Resolved X-ray Diffraction. *Can. Metall. Quart.*, vol. 23, pp. 121-130.

Garcı'a de Andre's, C.; Caballero, F.G.; Capdevila, C.; Bhadeshia, H.K.D.H. (1998): Modeling of isothermal ferrite formation using an analytical treatment of soft impingement in 0.37C1.45Mn-0.11V microalloyed steel. *Scripta Mater.*, vol. 39, pp. 853-859.

Gaude-Fugarolas, D.; Bhadeshia, H.K.D.H. (2003): A model for the austenitisation of hypoeutectoid steels. *J. Mater. Sci.*, vol. 38, pp. 1195-1201.

Grum, J.; Kek, T. (2004): The influence of different conditions of laser-beam interaction in laser surface hardening of steels. *Thin Solid Films*, vol. 453, pp. 94-99.

Hillert, M.; Nilsson, K.; Torndahl, L.E. (1971): Effect of alloying elements on the formation of austenite. *J. Iron Steel Inst.*, vol. 209, pp. 49.

Jacot, A.; Rappaz, M. (1998): A combined model for the description of austenitisation, homogenization and grain growth in hypo-eutectoid Fe-C steels during heating. *Acta Mater.*, vol. 47, pp. 1645-1651.

Jacot, A.; Rappaz, M.; Reed, R.C. (1998): Modeling of reaustenitization from the pearlite structure in steel. *Acta Mater.*, vol. 46, pp. 3949-3962.

Judd, R.R.; Paxton. H.W. (1968): Kinetics of austenite formation from a spherodised ferrite-carbide. *Trans. TMS-AIME.*, vol. 242, pp. 206-215.

Mioković, T.; Schulze, V.; Vöhringer, O.; Löhe, D. (2006): Prediction of phase transformations during laser surface hardening of AISI 4140 including the effects of inhomogeneous austenite formation. *Materials Science and Engineering: A*, vol. 435-436, pp. 547-555.

Molian P.A. (1989): Surface Alloying Using Lasers. In: T.S. Sudarshan (ed) *Surface modification technologies-An engineers guide*, Marcel Dekker, New York, p. 421.

Palmer, T.A.; Elmer, J.W. (2005): Direct Observations of the Formation and Growth of Austenite from Pearlite and Allotriomorphic Ferrite in a C-Mn Steel Arc Weld. *Scripta Mater.*, vol. 53, pp. 535-540.

Pantelis, D.I.; Bouyiouri, E.; Kouloumbi, N.; Vassiliou, P.; Koutsomichalis, A. (2002): Wear and corrosion resistance of laser surface hardened structural steel. *Surf. Coat. Technol.*, vol. 161, pp. 125-134.

Patankar, S.V. (1980): *Numerical Heat Transfer and Fluid Flow*. Hemisphere , New York.

Patwa, R.; Shin, Y.C. (2007): Predictive modeling of laser hardening of AISI5150H steels. *International Journal of Machine Tools and Manufacture*, vol. 47, no. 2, pp. 307-320.

Pashby, I.R.; Barnes, S.; Bryden, B.G. (2003): Surface hardening of steel using a high power diode laser. *Journal of Materials Processing Technology*, vol. 139, no. 1-3, pp. 585-588.

Roberts, G.A.; Mehl, R.F. (1943): The mechanism and the rate of formation of austenite from ferrite-cementite aggregates. *Trans. ASM.*, vol. 31, pp. 613-650.

Roósz, A.; Gácsi, Z.; Fuchs, E.G. (1983): Isothermal Formation of Austenite in eutectoid Plain Carbon Steel. *Acta Metall.*, vol. 31, pp.509-517.

Roy, A.; Manna, I. (2000): Mathematical modeling of localized melting around graphite nodules during laser surface hardening of austempered ductile iron. *Optics and Lasers in Engineering*, vol. 34, no. 4-6, pp. 369-383.

Sarkar, S.; Chakraborty, S. (2002): Three Dimensional Computational Modeling of Momentum, Heat and Mass Transfer in Laser Surface Alloying Process. *Numerical Heat Transfer*, vol. 42A, pp. 307-326.

Senthil, S.J.; Subramanian, K.; Nath, A.K. (1999): Effect of laser surface hardening on En18 (AISI 5135) steel. *J. Mater. Processing Technol.*, vol. 91, pp. 29-36.

Shin, H.J.; Yoo, Y.T.; Ahn, D.G.; Im, K. (2007): Laser surface hardening of S45C medium carbon steel using ND:YAG laser with a continuous wave. *Journal of Materials Processing Technology*, vol. 187-188, pp. 467-470.

Speich, G.R.; Demarest, V.A.; Miller, R.L. (1981): Formation of Austenite during inter-critical cooling of dual-phase steels. *Metall. Trans.*, vol. 12A , pp.1419-1428.

Speich, G.R.; Szirmae, A. (1969): Formation of. austenite from ferrite and ferrite-carbide aggregates. *Trans. TMS-AIME.*, vol. 245, pp. 1063-1074.